Volume 14, Issue 3, Page 120-129, 2025 https://doi.org/10.46810/tdfd.1615276 Research Article

BİNGÖL UNIVERSITY

Türk Doğa ve Fen Dergisi
Turkish Journal of Nature and Science
www.dergipark.gov.tr/tdfd

A New Model for Transmission Line Modelling Method to Investigate Frequency-Dependent Bioelectromagnetic Interactions

Burak ARICIOĞLU[1*], Abdullah FERİKOĞLU (Retired)[1]

[1] Sakarya University of Applied Sciences, Faculty of Technology, Electrical & Electronics Engineering Department, Sakarya, Türkiye
Burak ARICIOĞLU ORCID No: 0000-0001-9526-7629
Abdullah FERİKOĞLU ORCID No: 0000-0002-5907-1845

**Corresponding author: baricioglu@subu.edu.tr*

(Received: 08.01.2025, Accepted: 09.08.2025, Online Publication: 26.09.2025)

Keywords
TLM,
Skin depth,
SAR

Abstract: In this article, a new transmission line model is presented for the frequency-dependent analysis of bioelectromagnetic interactions. For the frequency-dependent analysis, the transmission line is modelled with dependent voltage sources in PSpice, allowing the transmission line lumped parameters to be defined as functions of frequency. This approach enables frequency-dependent analysis with a single simulation. As an example, the frequency-dependent electric field distribution in a multilayer human tissue model over the frequency range of 1 GHz to 100 GHz is investigated. The multilayer tissue model consists of skin, fat, and muscle layers. A finite element method (FEM)-based analysis of the electric field distribution in the multilayer tissue model is also conducted at the resonant frequency of the model, determined in this study to be 10.44 GHz. The transmission line modelling (TLM) and FEM-based results are in good agreement. Additionally, the skin depth of the multilayer tissue model is calculated. The results from both the electric field distribution analysis and the skin depth calculation confirm the accuracy of the proposed frequency-dependent transmission line model. Finally, the study examines the frequency-dependent electromagnetic energy absorption in the multilayer tissue model over the 1 GHz to 100 GHz frequency range.

İletim hattı modelleme yöntemi ile frekansa bağlı biyoelektromanyetik etkileşim için yeni bir model tasarımı

Anahtar Kelimeler
İHM,
Deri kalınlığı,
ÖSO

Öz: Bu makalede biyoelektromanyetik etkileşimlerin frekansa bağlı analizi için yeni bir iletim hattı modeli sunulmaktadır. Frekansa bağlı analiz için iletim hattı, PSpice programında bağımlı voltaj kaynaklarıyla modellenerek iletim hattı toplu parametrelerinin frekansa bağlı fonksiyonlar olarak tanımlanmıştır. Bu yaklaşım ile tek bir simülasyonla frekansa bağlı analiz gerçekleştirilebilir. Örnek olarak çok katmanlı bir insan doku modelinde 1 GHz ile 100 GHz frekans aralığı için frekansa bağlı elektrik alan dağılımı incelenmiştir. Çok katmanlı doku modeli deri, yağ ve kas katmanlarından oluşmaktadır. Yapılan analizde modelin rezonans frekansı 10,44 GHz olarak belirlenmiştir. Bu frekans için sonlu elemanlar yöntemi ile analiz gerçekleştirilmiştir. İletim hattı modelleme (İHM) ve sonlu eleman yöntemleri ile elde edilen sonuçlar oldukça uyumlu olduğu gözlemlenmiştir. Ayrıca çok katmanlı doku modelinde deri kalınlığı hesaplanmıştır. Simülasyondan ve hesaplamadan elde edilen deri kalınlığı değerleri birbiriyle uyumlu olduğu gözlemlenmiştir. Bu da önerilen iletim hattı modelinin başarımını göstermektedir. Son olarak çalışma, 1 GHz ila 100 GHz frekans aralığında çok katmanlı doku modelinde frekansa bağlı elektromanyetik enerji emilimini incelenmiştir.

1. INTRODUCTION

The study of electromagnetic (EM) wave interactions with biological systems is a critical and evolving field, driven by the pervasive use of wireless technologies, advancements in medical diagnostics, and therapeutic applications. Understanding these interactions, particularly at high frequencies, is essential for both safety assessment and the development of novel biomedical technologies. The fundamental description of all electromagnetic phenomena is encapsulated in Maxwell's equations. However, obtaining of an analytic solution to Maxwell's equations is not easy in most cases. Numerous numerical techniques have been developed to solve these equations. The most widely used methods include the finite element method (FEM) [1], the method of moments (MoM) [2], the finite-difference time-domain technique (FDTD) [3], the finite integration technique (FIT) [4], the method of lines (MoL) [5], and the transmission line modelling (TLM) method [6]. These numerical methods differ in several aspects, such as their applicable domains (some are suited only for time or frequency domains, while others can handle both), their discretization approaches, their model boundaries, and their capability to be applied to nonlinear complex media [7].

Table 1. Comparative overview of some numerical methods in computational electromagnetics

Method	Primary Domain	Discretization Approach	Key Strengths	Key Limitations
FEM	Frequency	Volume-based	Handles complex geometries, multi-physics coupling, no numerical dispersion (FD), guaranteed convergence [8]	Computationally expensive (volumetric meshing), complex meshing, steeper learning curve [8]
MoM	Frequency	Surface-based	Efficient for open regions/scattering, surface meshing, no numerical dispersion [9]	Computationally intensive (dense matrices), limited to linear/homogeneous media, convergence not guaranteed, harder to parallelize [9]
FDTD	Time	Volume-based	Conceptual simplicity, broadband analysis from single run (with FFT), handles nonlinearity, guaranteed convergence [10]	Global grid issues for complex geometries, numerical dispersion error (accumulates), CFL condition constraint [10]
TLM	Time (adaptable to Frequency)	Network/ Circuit-based	Unconditional stability, intuitive visualization, material/mesh flexibility, computational efficiency (parallelizable), complex/nonlinear/dispersive material handling, better boundary geometry modeling [11]	Higher memory per node, early 3D complexity [11]
FIT	Time/ Frequency	Volume-based	Stability and discretization of Maxwell's equations in their integral form. [12]	Poor performance in transverse scaling, complex implementation [12]
MoL	Time/ Frequency	Line-based	Suitable for longitudinally repeating objects and resonant structures. [13]	The scaling performance in the transverse direction is very poor, it is somewhat difficult to visualize. [13]

TLM is, firstly, used by G. Kron [14,15] as an equivalent circuit representation of Maxwell's equations. P. B. Johns and R. L. Beurle introduce a numerical method based on Kron's equivalent circuit representation with impulse excitation of the circuit [16]. Some features of TLM, which explain why it is preferred in computational electromagnetics [11] can be listed as:

- It is unconditionally stable.
- It allows easy visualization of the problem being simulated.
- It supports variable mesh size and material.
- Its numerical solution is simple and can be easily parallelized.

PSpice is a general-purpose circuit simulator. It is capable of handling analog, logical, and mixed-signal components, circuits, and systems. There are studies in the literature where electromagnetic problem solved in PSpice environment based on TLM method. For instance, in [17], the transmission line model of PSpice is employed to simulate wave propagation in a lossless medium. Similarly, in [18], the same model is used to compute the voltage standing wave ratio (VSWR) for various types of terminations. In [19], a one-dimensional multilayered planar tissue model is used to investigate electromagnetic energy absorption when the model is exposed to radiation from a base-station antenna for two different frequencies. However, as seen in the aforementioned studies, traditional implementations often assume frequency-independent parameters or rely on repeated simulations across discrete frequencies, limiting their applicability in broadband scenarios within PSpice environment.

This study addresses that gap by developing a frequency-dependent TLM framework implemented in PSpice using dependent voltage sources (ELaplace devices). This approach allows the lumped parameters of the transmission line—resistance, inductance, capacitance, and conductance—to be explicitly defined as functions of frequency.

In this study, a one-dimensional (1D) multilayer planar tissue model was employed to investigate electromagnetic energy absorption using the TLM method. Previous studies have analysed electromagnetic energy absorption in tissues using various models [20–23]. In this work, the stratification model of tissues was selected as skin, fat, and muscle, as described in [24–27]. A simulation was performed for frequencies ranging from 1 GHz to 100

GHz, assuming far-field radiation conditions, and its performance is validated through comparison with FEM-based analysis and theoretical skin depth calculations
The structure of the paper is as follows: Section 2 describes the materials and methods, Section 3 presents the simulations and results, and Section 4 offers a conclusion.

2. MATERIAL AND METHOD

2.1. Material and Method Subheading

In this study, a one-dimensional (1D) multilayer human tissue model is used for simulations. The solution of the field equations for a plane wave traveling through a medium is analogous to the solution of a voltage wave on a transmission line.

Consider a plane wave propagating in the z-direction within a lossy medium. The field equation for a transverse electromagnetic (TEM) wave can be expressed as:

$$\nabla^2 E - \gamma^2 E = 0 \tag{1}$$

where

$$\gamma^2 = j\omega\mu(\sigma + j\omega\varepsilon) \tag{2}$$

In Equation 2, ω represents angular frequency, and μ, σ, and ε represent field parameters permeability, conductivity, and permittivity, respectively.

The solution of Equation 1 can be written as:

$$E_x(z) = E_0 e^{-\gamma z} + E_0' e^{\gamma z} \tag{3}$$

where E_0 and E_0' represent the magnitude of the incident and reflected electric field, respectively.

Similarly, the equation of a voltage wave on a transmission line can be written as:

$$\nabla^2 V - \gamma^2 V = 0 \tag{4}$$

where

$$\gamma^2 = (j\omega L + R)(j\omega C + G) \tag{5}$$

In Equation 5, ω represents angular frequency, and L,R,C and G represent transmission line parameters inductance, resistance, capacitance, and conductance per meter, respectively.

The solution of Equation 4 can be written as:

$$V_x(z) = V_0 e^{-\gamma z} + V_0' e^{\gamma z} \tag{6}$$

Where V_0 and V_0' represent the magnitude of the incident and reflected voltage wave, respectively.

Finally, the intrinsic impedance of a lossy medium is,

$$\eta = \sqrt{\frac{j\omega\mu}{\sigma + j\omega\epsilon}} \tag{7}$$

and, the corresponding characteristic impedance of a lossy line is,

$$Z_0 = \sqrt{\frac{R + j\omega L}{G + j\omega C}} \tag{8}$$

As evident from the equations above, the solution for an electromagnetic wave traveling through a medium is mathematically equivalent to that of a voltage wave traveling through a transmission line. For this equivalence to hold, the medium's parameters μ (permeability), σ (conductivity), and ε (permittivity) must correspond to the transmission line's parameters L (inductance meter $^{-1}$), G (conductance meter $^{-1}$), and C (capacitance meter $^{-1}$), respectively. Additionally, the value of R (resistance meter $^{-1}$) in the transmission line must be set to zero, as there is no analogous parameter for R in the medium.

2.2. Frequency-Dependent Transmission Line Model

In this section, the transmission line model for frequency-dependent parameters is described. The currents at both ends of a transmission line, shown in Figure 1a, can be expressed as below [28]:

$$\begin{aligned} i_a &= \frac{V_a}{Z_0} - i_b' \\ i_b &= -\frac{V_b}{Z_0} + i_a' \end{aligned} \tag{9}$$

where Z_0 is the characteristic impedance of the transmission line discussed in the previous section, and i_a' and i_b' are described as:

$$\begin{aligned} i_a' &= i_a e^{-\gamma l} + \frac{V_a}{Z_0} e^{-\gamma l} \\ i_b' &= i_b e^{-\gamma l} + \frac{V_b}{Z_0} e^{-\gamma l} \end{aligned} \tag{10}$$

where γ is the propagation constant of the line, as described in Equation 5.

Using Equation 9, the Thevenin model of a transmission line link can be implemented as shown in Figure 1b.

The Thevenin model given in Figure 1b can be implemented in PSpice with an 'ELaplace' device for frequency-dependent simulations. The impedances in Figure 1b can also be modelled with the 'ELaplace' device.

In Figure 2, the PSpice implementation of the Thevenin model is given. All the sources in the figure are dependent voltage sources. Among the sources, V_{a1},V_{a3},V_{b1}, and V_{b3} are current controlled voltage sources with gain Z_0, $Z_0 e^{-\gamma l}$,Z_0, and $Z_0 e^{-\gamma l}$, respectively, while V_{a2} and V_{b2} are voltage controlled voltage sources with gain $e^{-\gamma l}$.

These dependent voltage sources are implemented in PSpice with 'ELaplace' devices, in which the gains of these sources can be defined in terms of frequency, and the 'ELaplace' device can be either a current or voltage-controlled voltage source. The PSpice expression of Figure 2 is given in Appendix B. An example of a PSpice expression of a frequency-dependent transmission line cell for tissue is provided in Appendix C.

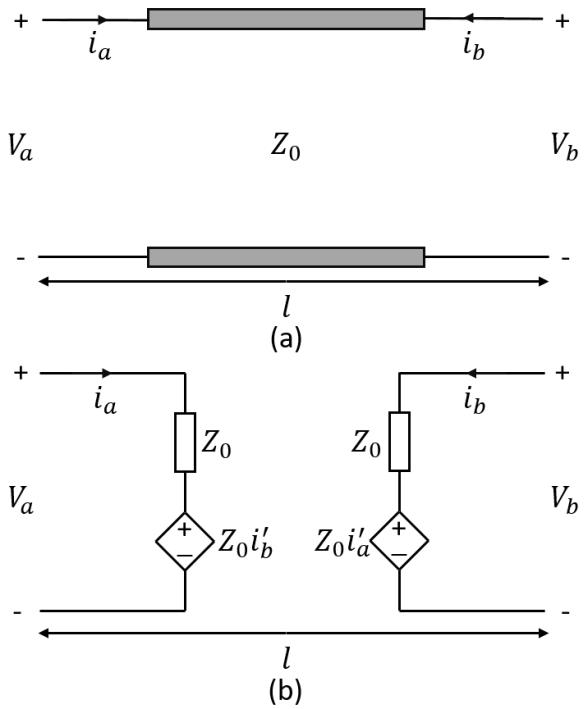

Figure 1. (a) Transmission line and **(b)** its Thevenin model

.

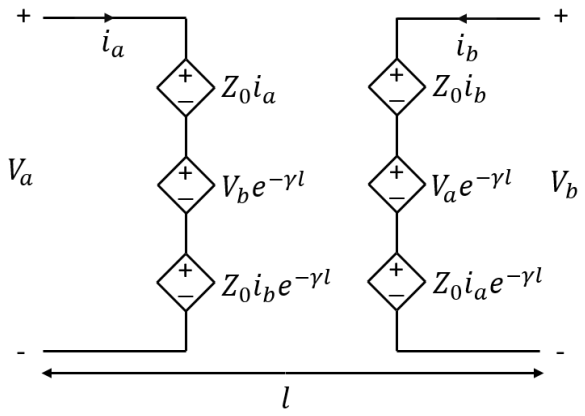

Figure 2. PSpice implementation of transmission line Thevenin model

2.3. The Multilayer Human Tissue Model Used in Simulations

The multilayer human tissue model used in this study is depicted in Figure 3. The model consists of three layers: skin, fat, and muscle tissues. For the simulations, the thicknesses of the skin, fat, and muscle layers were set to 1 mm, 4 mm, and 10 mm, respectively, as specified in [29].

The TLM method is used to analyse electric field distribution in multilayer tissue. A transmission line model is generated for each tissue layer since the medium parameters are different for each tissue. Each layer is further subdivided into 100 identical transmission line cells, as illustrated in Figure 4. The frequency-dependent parameters, namely C and G of the transmission line, were defined as a function of frequency.

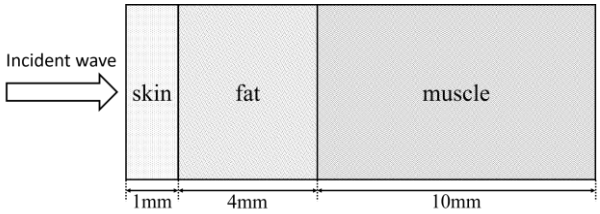

Figure 3. Multilayer tissue model used in the study

The lengths of the transmission line cells are 10^{-2} mm for skin, 4 x 10^{-2} mm for fat, and 10^{-1} mm for muscle tissue. In Figure 4, the transmission line cells depicted as TSi, TFi, and TMi represent skin, fat, and muscle tissues, respectively, Z_{air} is intrinsic impedance of air (377Ω), independent of frequency, and Z_L is the intrinsic impedance of muscle tissue, which is frequency-dependent

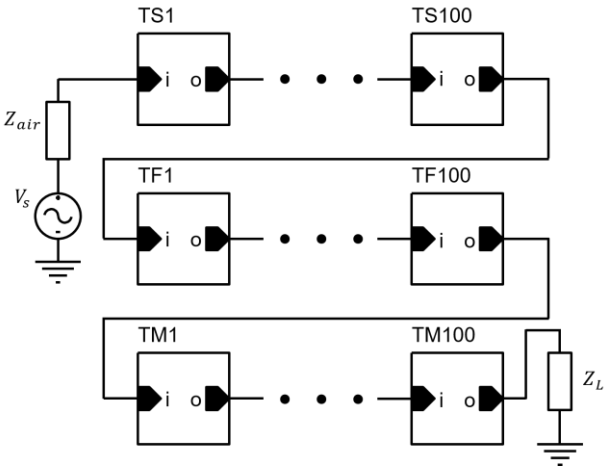

Figure 4. PSpice schematic for the simulation of electric field distribution in the multilayer tissue model, TSi, TFi, and TMi represent skin, fat, and muscle tissues respectively

Z_L is selected as the intrinsic impedance of muscle tissue to prevent waves from being reflected back at the end of the muscle tissue. Since Z_L is frequency-dependent, an 'ELaplace' device is used to emulate a frequency-dependent impedance. The general expression of 'ELaplace' is:

"E{name} {+node} {-node} LAPLACE {expression} {s expression} "

An example PSpice expression for frequency-dependent impedance is given in Appendix A.

As mentioned in the previous section, L, G, and C parameters of the line are equivalent to μ, σ, and ε parameters of the medium, respectively. Among the medium parameters, σ and ε parameters vary with frequency, while μ parameter does not, since human tissues are a non-magnetic material that their magnetic

permeability (μ) is the same as or very close to that of vacuum [30–33]. In Figure 5, relative permittivity (ε_R) and conductivity (σ) of tissues are given for a frequency range of 1 GHz-100 GHz.

In order to perform an AC analysis of the multilayer tissue, some of the transmission line parameters, namely C and G, should be defined as a function of frequency. As a first step, for each curve in Figure 5, a frequency-dependent polynomial is constructed using the curve fitting method.

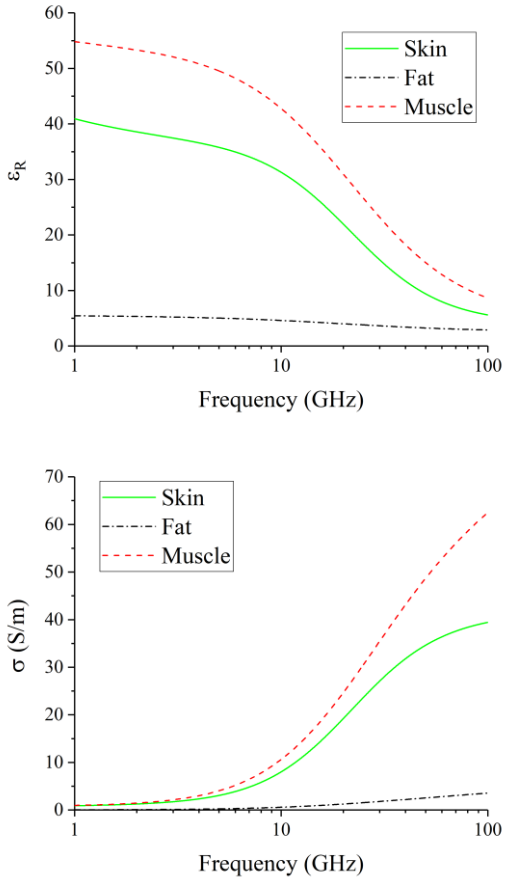

Figure 5. Relative permittivity (above) Conductivity of the tissues (bottom) used in the study with respect to frequency

The process for defining frequency-dependent parameters in PSpice involves modelling a frequency-dependent transmission line, which was detailed in the previous section.

3. SIMULATIONS AND RESULTS

In the analysis of electric field intensity distribution in the multilayer tissue model for the frequency range of 1 GHz-100 GHz, the root mean square (RMS) value of the incoming electric field is set as 1 V m^{-1}. The normalized electric field distribution is given in Figure 6.

As shown in Figure 6, at certain frequencies, the electric field magnitude exceeds that of the incoming electric field. The maximum occurs at approximately 10.44 GHz, where the electric field magnitude nearly doubles that of the incoming field. In this study, the human tissue modelled as a multilayer with each layer having different electrical properties. Because of this, there will be multiple reflections. Other than reflections, there will be phase changes and standing wave effects. The electric field strength, shown in Figure 6, takes into account the aforementioned effects. Because of these effects, the magnitude of the electric field may increase as it travels through the multilayer medium [34]. Similar results were found in [34-39] where the magnitude of the electric field increased as it travelled through multilayer tissue model. However, in all these studies, the frequency at which this phenomenon occurs is different since the number of layers in the multilayer tissue model and the thickness of each tissue are different from the model employed in this study.

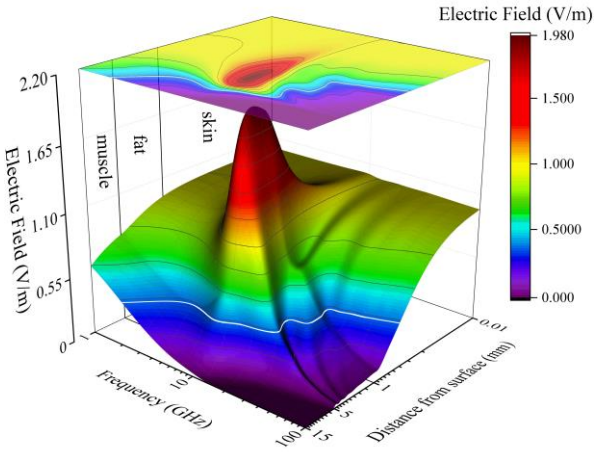

Figure 6. The normalized electric field distribution in the multilayer tissue model for the frequency range 1GHz – 100 GHz

To further investigate this phenomenon, the equivalent characteristic impedance of the multilayer tissue is analysed, as it can be related to the resonant frequency. The input impedance of a transmission line can be written as:

$$Z_{in} = Z_0 \frac{Z_L + Z_0 \tanh(\gamma l)}{Z_0 + Z_L \tanh(\gamma l)} \quad (11)$$

where Z_0 is the characteristic impedance of the line, as described in Equation 8. Z_L is the load impedance of the line, γ is the propagation constant, as described in Equation 5, and l is the length of the line.

Accordingly, the equivalent characteristic impedance of the multilayer tissue can be written as:

$$Z_{eq} = Z_{0_s} \frac{Z_{L_s} + Z_{0_s} \tanh(\gamma_s l_s)}{Z_{0_s} + Z_{L_s} \tanh(\gamma_s l_s)} \quad (12)$$

where Z_{0_s}, γ_s, and l_s are the characteristic impedance, propagation constant, and the length of skin tissue, respectively. Z_{L_s} is the load seen by the skin tissue, which is equal to the input impedance of the fat tissue and can be written as:

$$Z_{L_s} = Z_{0_f} \frac{Z_{0_m} + Z_{0_f} \tanh(\gamma_f l_f)}{Z_{0_f} + Z_{0_m} \tanh(\gamma_f l_f)} \quad (13)$$

where Z_{0_f}, γ_f, and l_f are the characteristic impedance, propagation constant, and the length of the fat tissue, respectively, and Z_{0_m} is the characteristic impedance of the muscle tissue. The load seen by the fat tissue is equivalent to the characteristic impedance of the muscle tissue, as the muscle tissue is terminated with a perfectly matched layer (PML).

The magnitude, real, and imaginary parts of the equivalent impedance of the multilayer tissue are given in Figure 7 with respect to frequency.

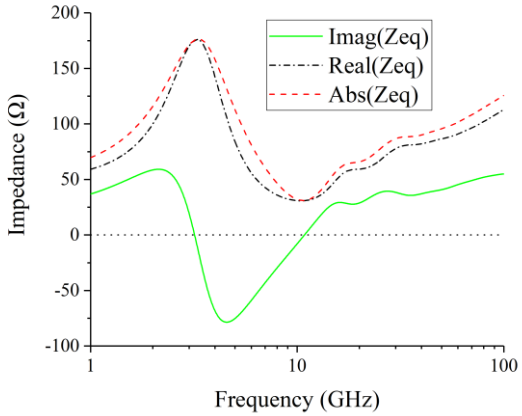

Figure 7. The magnitudes of absolute, real part, and imaginary part of the multilayer tissue model equivalent impedance with respect to frequency

If Figure 7 is examined, the imaginary part of the equivalent impedance is zero at two frequencies, 3.83 GHz and 10.44 GHz. In other words, at these two frequencies the equivalent impedance is purely resistive. The resonant frequency can be described as the frequency at which the equivalent impedance of a circuit has no imaginary part. Hence, 3.83 GHz and 10.44 GHz are the two resonant frequencies of the multilayer tissue model used in this study. As can be seen in Figure 7, the real part is minimum at 10.44 GHz while it has a maximum at 3.83 GHz. Since the real part of the equivalent impedance at 10.44 GHz has a minimum, a maximum peak electric field occurs at this frequency.

Finite element method (FEM)-based analysis of electric field distribution in the multilayer human tissue at 10.44 GHz is conducted to compare the result of transmission line modelling (TLM) method analysis at this frequency. The results of both methods at 10.44 GHz are given in Figure 8. As can be seen in the figure, the results of both methods are very close to each other. This shows the successful performance of the proposed transmission line.

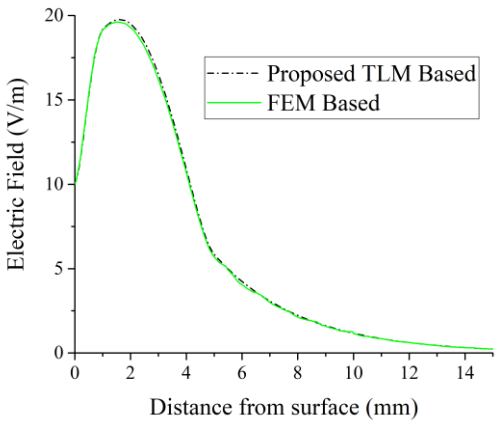

Figure 8. FEM and TLM-based analysis of electric field distribution in the multilayer tissue model at the resonant frequency of 10.44 GHz

To evaluate the results of TLM-based analysis, the skin depth of the multilayer tissue is also calculated over the frequency range 1 GHz – 100 GHz, and both results are compared.

For an N-layer medium, effective skin depth can be calculated as [40]:

$$\delta_{eff} = \sum_{i=1}^{N+1} d_i$$

$$d_i = \int_{\sum_{j=1}^{i-1} l_j}^{\sum_{j=1}^{i} l_j} \left| \frac{\prod_{j=1}^{i-1}(1+\Gamma_j)}{\prod_{j=1}^{i}(e^{\gamma_j}+\Gamma_j e^{-\gamma_j})} \left(e^{-\gamma_i (z-\sum_{j=0}^{i-1} l_j)} + \Gamma_i e^{\gamma_i (z-\sum_{j=0}^{i} l_j)} \right) \right| dz \qquad (14)$$

$$d_{N+1} = \int_{\sum_{j=1}^{N} l_j}^{\infty} \left| \frac{\prod_{j=1}^{N}(1+\Gamma_j)}{\prod_{j=1}^{N}(e^{\gamma_j}+\Gamma_j e^{-\gamma_j})} (e^{-\gamma_i (z-\sum_{j=0}^{N+1} l_j)}) \right| dz$$

where δ_{eff} is the effective skin depth, d_i contribution of each layer to the effective skin depth, and Γ_i, γ_i and l_i are the reflection coefficient, the propagation constant and the length of the i^{th} layer, respectively. The calculated effective skin depth of the multilayer tissue is given in Figure 9.

Skin depth can be simply defined as the depth at which the current density has fallen to 1/e (about 0.37) of surface current density. Since

$$J = \sigma E \qquad (15)$$

where J is the current density, σ is conductivity, and E is the electric field, skin depth can be redefined as the depth at which the electric field magnitude has fallen to e^{-1} (about 0.37) of the electric field magnitude at the surface of the medium.

In Figure 9, skin depth in the TLM-based analysis is obtained from Figure 6 by plotting distance at which the electric field magnitude has fallen to e^{-1} of the incoming electric field against frequency. In Figure 6, the white line shows the skin depth.

If Figure 9 is examined, it can be said that the calculated skin depth result confirms that of TLM-based analysis. However, the two results are not very close to each other because, in TLM-based analysis, the field parameters are constructed with curve fitting.

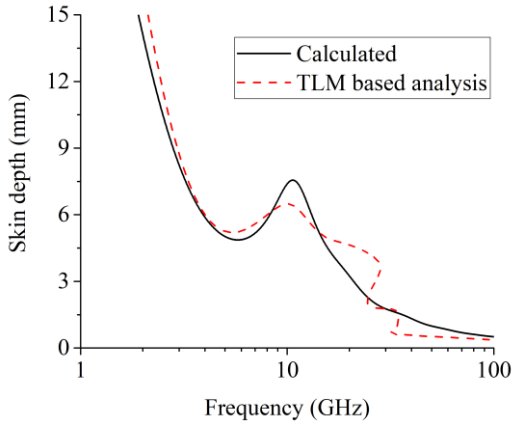

Figure 9. Calculated effective skin depth and skin depth obtained from TLM-based analysis with respect to frequency

It is stated that in [34, 37, 41-43], at higher frequencies (above 30 GHz), the electromagnetic waves have a smaller penetration depth typically on the millimetre (mm) order. This is also observed in this study, as shown in Figure 9, where the skin depth above 30 GHz is less than 1 mm. It is also found that the skin depth is less than 1 mm above 30 GHz in [34, 37]

Finally, specific absorption rate (SAR) of the multilayer tissue is calculated for the frequency range 1GHz-10GHz. SAR can be expressed as:

$$SAR = \frac{\sigma}{\rho} E_{rms}^2 \tag{16}$$

where σ and ρ represent conductivity and density of tissue, and E_{rms} is the RMS value of the electric field.

The average SAR of the multilayer tissue for the frequency range 1 GHZ-100 GHz is given in Figure 10. For the SAR value calculation, the magnitude of the incident electric field at the surface of the tissue model is 1 V m^{-1} (RMS). If the magnitude of the incident fields is doubled, then the SAR value is quadrupled since SAR is squarely proportional to the magnitude of the electric field.

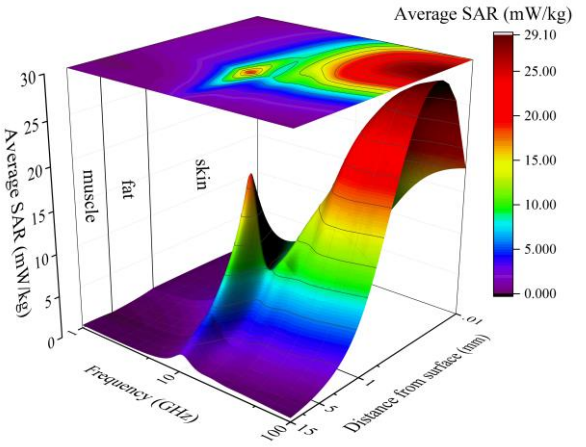

Figure 10. The average SAR of the multilayer tissues model with respect to both distance and frequency for the normalized electric field

If Figure 10 is examined, the local maximum SAR is observed at the largest frequency in the skin tissue since SAR is proportional to conductivity and squarely proportional to the electric field. However, the maximum average SAR is observed at the resonant frequency of the multilayer tissue model, since the magnitude of the electric field at that frequency is the highest. Also, at all the frequencies the maximum local SAR is observed near the surface of the skin tissue at the incident wave side except for the frequencies in the neighbourhood of the resonant frequency 10.44 GHz. In the latter frequencies, the maximum local SAR is observed at the other end of the skin tissue, near the fat tissue.

4. CONCLUSION

The accurate modelling of electromagnetic wave interactions with biological tissues is a cornerstone of modern bioelectromagnetic, driven by the complexities of human anatomy and the pervasive nature of electromagnetic fields in daily life and medical applications. The inherent heterogeneity, anisotropy, and frequency-dependent dielectric properties of biological media fundamentally limit the utility of analytical solutions to Maxwell's Equations, necessitating the adoption of sophisticated numerical techniques.

The present work contributes to the literature by introducing a novel TLM implementation that leverages the capabilities of the circuit simulation software, PSpice, to perform frequency-dependent analysis. The employment of dependent voltage sources (ELaplace devices, which can be defined as a function of frequency) allows for the direct definition of frequency-dependent lumped parameters, enabling a comprehensive broadband analysis in a single simulation run. This approach offers significant computational efficiency compared to traditional frequency sweeps.

A TLM-based frequency-domain analysis of a multilayer tissue model is conducted. To validate the proposed approach, several additional analyses are performed. The resonant frequencies of the multilayer tissue model are identified by examining the imaginary part of the characteristic impedance. It is found that, at one of the resonant frequencies (10.44 GHz), the electric field

distribution is maximized. Subsequently, a FEM-based electric field distribution analysis is carried out at this frequency, yielding results that closely match those of the TLM-based analysis. In a final analysis, the skin depth of the multilayer tissue is calculated, and the skin depth obtained from the TLM-based analysis is found to be in agreement with the theoretical calculation.

Following these analyses, the average SAR values for the frequency range 1 GHz to 100 GHz are calculated using the electric field distributions from the TLM-based analysis. As the frequency increases, the maximum local SAR value rises, primarily near the surface of the skin tissue. However, the highest average SAR is observed at the resonant frequency of the multilayer tissue model. At this resonant frequency (10.44 GHz), the maximum local SAR is observed at the far end of the skin tissue. Future studies will focus on frequency analysis of other human tissues, such as ocular tissue, and will explore temperature distribution in tissues induced by the electric field.

REFERENCES

[1] Zhang J, Jin J, Li X, Feng F, Liu W, Zhang W, et. al. A Novel Design Space Decomposition Technique to Accelerate FEM-Based Electromagnetic Topology Optimization for Waveguide Structures. IEEE Transactions on Microwave Theory and Techniques. 2024.

[2] Chai SR, Meng LH, Zou YF, Dai PK. Fast Computation of EM Scattering from Moving PEC Target Based on MT-ACA-MoM Algorithm. IEEE Antennas and Wireless Propagation Letters. 2024.

[3] Ball JM, Li W. Using high-resolution microscopy data to generate realistic structures for electromagnetic FDTD simulations from complex biological models. Nature Protocols. 2024; 1-33.

[4] Lin G, Huang T, Cai W, Gong D, Jin X. An Efficient Scheme of Waveguide Port Modeling Based on Conformal and Nonuniform Mesh for Time Domain Finite Integration Technique. IEEE Transactions on Antennas and Propagation. 2024.

[5] Wang X, Huang B. Analysis of conductor losses of planar transmission lines with surface roughness by the method of lines. Applied Computational Electromagnetics Society Symposium (ACES), 2017; p.1-2.

[6] Johns PB, Beurle RL. Numerical solutions of 2-dimentional scattering problems using a transmission-line matrix. Proc IEEE. 1971; 118(9): 1203-1208.

[7] Park S, Kotzev M, Brüns HD, Kam DG, Schuster C. Lessons from applying IEEE standard 1597 for validation of computational electromagnetics computer modeling and simulations. IEEE Electromagnetic Compatibility Magazine. 2017; 6(2): p.55-67.

[8] Sheng XQ, Song W. Essentials of computational electromagnetics. John Wiley & Sons. 2011.

[9] Ayari M, Gharbi A, El Touati Y, Klai Z, Elsayed MS. Advanced numerical methods in electromagnetics: techniques and applications. Letters in High Energy Physics. 2024; 791–803.

[10] Rylander T, Ingelström P, Bondeson A. Computational electromagnetics. Springer Science & Business Media. 2012.

[11] Duffy AP. The application of transmission-line modelling to EMC design. Does Electromagnetic Modelling Have A Place in EMC Design IEE Colloquium on IET. 1993.

[12] Weiland T. Finite integration method and discrete electromagnetism. In: Monk P, Carstensen C, Funken S, Hackbusch W, Hoppe RHW, editors. Computational Electromagnetics. Lecture Notes in Computational Science and Engineering, vol. 28. Springer, Berlin, Heidelberg. 2003.

[13] Schiesser WE. Method of lines PDE analysis in biomedical science and engineering. John Wiley & Sons. 2016.

[14] Kron G. Equivalent circuits to represent the electromagnetic field equations. Physical Review. 1943; (643)-4: 126.

[15] Kron G. Equivalent circuit of the field equations of Maxwell-I. Proceedings of the IRE 325. 1944; p.289-299.

[16] Peter JB, Beurle RL. Numerical solution of 2-dimensional scattering problems using a transmission-line matrix. Proceedings of the Institution of Electrical Engineers.1971; 118(9).

[17] Portnoy WM. PSPICE as a simulation tool in teaching electrodynamics. In: Technology-Based Re-Engineering Engineering Education, Proceedings of Frontiers in Education (FIE'96) 26th Annual Conference. IEEE. 1996; 1: 238–241.

[18] Tobin P. The role of PSpice in the engineering teaching environment. In: International Conference on Engineering Education – ICEE. 2007.

[19] Ferikoğlu A, Çerezci O, Kahriman M, Yener ŞÇ. Electromagnetic absorption rate in a multilayer human tissue model exposed to base-station radiation using transmission line analysis. IEEE Antennas and Wireless Propagation Letters. 2014; 13: 903–906.

[20] Curto S, Ammann MJ. Electromagnetic interaction between resonant loop antenna and simulated biological tissue. Microw Opt Techn Let. 2006; 48(12): 2418–2421.

[21] Zhang HH, Lin ZC, Wei EI, Choi WW, Tam KW, Donoro DG, et. al. Electromagnetic-thermal analysis of human head exposed to cell phones with the consideration of radiative cooling. IEEE Antennas and Wireless Propagation Letters.2018; 17(9): 1584-1587.

[22] Lee AK, Choi HD. Environmental EMF Evaluation for Mobile Communication Base Stations. 2021 XXXIVth General Assembly and Scientific Symposium of the International Union of Radio Science (URSI GASS) IEEE;2021. p. 1-2

[23] Karipidis K, Baaken D, Loney T, Blettner M, Brzozek C, Elwood M et.al. The effect of exposure to radiofrequency fields on cancer risk in the general and working population: A systematic review of human observational studies–Part I: Most researched outcomes. Environment International. 2024;108983.

[24] Wang H. Analysis of electromagnetic energy absorption in the human body for mobile terminals. IEEE Open Journal of Antennas and Propagation. 2020; 1: p. 113-117.
[25] Melia G. Electromagnetic absorption by the human body from 1-15 GHz (Doctoral dissertation) University of York, 2013.
[26] Maiorana E, Ramaccia D, Stefanini L, Toscano A, Bilotti F, Campisi P. Biometric Recognition Based on Hand Electromagnetic Scattering at Microwaves. IEEE Transactions on Microwave Theory and Techniques, 2023.
[27] Azzaz-Rahmani S, Zerrouki H, Dekkiche L. Novel Microstrip Patch Antenna for implantable medical telemetry devices. Journal of Applied Science and Engineering. 2021; 24(6): p.853-860.
[28] Moreno P, Ambrosio A, Gómez P. The characteristics approach for modeling single phase transmission lines with frequency dependent electrical parameters. Transmission and Distribution Conference and Exposition: Latin America 2008 IEEE/PES;2008. p. 1-4.
[29] Lin JC. Microwave propagation in biological dielectrics with application to cardiopulmonary interrogation. Medical applications of microwave imaging. 1986; p.47–58.
[30] Hennig A, vom Bogel G. Analysis of power absorption by human tissue in deeply implantable medical sensor transponders. Advanced Microwave Circuits and Systems. 2010.
[31] Schwan HP, Foster KR. RF-field interactions with biological systems: electrical properties and biophysical mechanisms. Proceedings of the IEEE. 1980; 68(1): p.104–113.
[32] Barchanski A. Simulations of low-frequency electromagnetic fields in the human body. (Phd thesis) Berlin: Technische Universitt; 2007
[33] Stuchly MA. Biological Effects of Electromagnetic Fields. International Journal of Bioelectromagnetism. 2002; 14(2): p.157–160
[34] Ziskin MC, Alekseev SI, Foster KR, Balzano Q. Tissue models for RF exposure evaluation at frequencies above 6 GHz. Bioelectromagnetics. 2018; 39(3): 173–189.
[35] Gustrau F, Bahr A. W-band investigation of material parameters, SAR distribution, and thermal response in human tissue. IEEE Transactions on Microwave Theory and Techniques. 2002; 50(10): 2393–2400.
[36] Sabbah AI, Dib NI, Al-Nimr MA. Evaluation of specific absorption rate and temperature elevation in a multi-layered human head model exposed to radio frequency radiation using the finite-difference time domain method. IET Microwaves, Antennas & Propagation. 2011; 5(9): 1073–1080.
[37] Kaburcuk F, Elsherbeni AZ, Lumnitzer R, Tanner A. Electromagnetic waves interaction with a human head model for frequencies up to 100 GHz. Applied Computational Electromagnetics Society Journal (ACES). 2020; 613–621.
[38] Grund J, Rathjen KU, Rädel C, Stiemer M, Dickmann S. Planar multilayer model of human tissue exposed to a plane electromagnetic wave. IEEE Journal of Electromagnetics, RF and Microwaves in Medicine and Biology. 2020; 5(4): 305–312.
[39] Laganà F, Bibbò L, Calcagno S, De Carlo D, Pullano SA, Pratticò D, Angiulli G. Smart electronic device-based monitoring of SAR and temperature variations in indoor human tissue interaction. Applied Sciences. 2025; 15(5): 2439.
[40] Hong-Wei D. et. al. Effective skin depth for multilayer coated conductor. Progress In Electromagnetics Research. 2009; p.1-8.
[41] Kanezaki A, Hirata A, Watanabe S, Shirai H. Effects of dielectric permittivities on skin heating due to millimeter wave exposure. BioMedical Engineering OnLine. 2009; 8(1): 20.
[42] Christ A, Samaras T, Neufeld E, Kuster N. RF-induced temperature increase in a stratified model of the skin for plane-wave exposure at 6–100 GHz. Radiation Protection Dosimetry. 2020; 188(3): 350–360.
[43] Kaburcuk F. Effect of skin thickness on electromagnetic dosimetry analysis of a human body model up to 100 GHz. International Journal of Microwave and Wireless Technologies. 2024; 16(8): 1373–1380.

Appendices

Appendix A. An exemplary PSpice expression for frequency-dependent impedance

```
 E_IMP n+ n- LAPLACE {i(vL)} {
*real part of the impedance
++pre1*(abs(s) + pre0
*imaginary part of the impedance
++(s*(pl1*abs(s) + pl0))}
```

where i(vL) is the current flown through the impedance, pre1, pre0, pl1, and pl0 are the parameters are obtained from curve fitting. s is the complex angular frequency $s = j\omega$ and abs(.) is the absolute value function.

Appendix B. The PSpice expression of the frequency-dependent transmission line model

```
.subckt tlossyline_thevenin_model A1 A2 B1 B2 params:
len=1 R=1 L=1 G=1 C=1
EA1 A1 1 laplace {i(EA1)} = {sqrt((L*s+R)/(C*s+G))}
EA2 1 2 laplace {v(B1,B2)} =
+{exp(-len*sqrt((L*s+R)*(C*s+G)))}
EA3 2 3 laplace {i(EB1)} =
+{exp(-len*sqrt((L*s+R)*(C*s+G)))
+*sqrt((L*s+R)/(C*s+G))}
R1 3 A2 50n

EB1 B1 4 laplace {i(EB1)} = {sqrt((L*s+R)/(C*s+G))}
EB2 4 5 laplace {v(A1,A2)} =
+{exp(-len*sqrt((L*s+R)*(C*s+G)))}
EB3 5 B2 laplace {i(EA1)} =
+ {exp(-len*sqrt((L*s+R)*(C*s+G)))
+*sqrt((L*s+R)/(C*s+G))}
.ends
```

There is an extra resistor element 'R1' to break the voltage source loop in the simulation. If the value of 'R1' is selected R1$\ll Z_0$, then the effects of resistor 'R1' can be omitted.

Appendix C. An example PSpice expression of frequency-dependent transmission line cell for skin tissue

```
.subckt Tskin  A1  A2  B1  B2 params: len=0.1e-4
****conductivity curve*****
.param pc0 {4.5546e-09}
.param pc1 {3.2281e-09}
****relative permittivity curve****
.param pr0 {0.0008023}
.param pr1 {0.0057397}
.param eps0 {8.854e-12}
xlossydskin A1 A2 B1 B2 tlossyline_thevenin_model params: len={len}
****here the lumped elements can be defined as a function of angular frequency abs(s)=ω=2πf)
+          r={0}
+          l={1.257u}
+          g={ pc1*abs(s) + pc0}
+          c={eps0*(pr1*abs(s) + pr0)}
.ends.
```